energies

MDPI

Article

Analysis of Shielding Properties of Head Covers Made of Conductive Materials in Application to 5G Wireless Systems

Łukasz Januszkiewicz

Institute of Electronics, Lodz University of Technology, Al. Politechniki 10 Street, 93-590 Lodz, Poland; lukasz.januszkiewicz@p.lodz.pl; Tel.: +48-42-6312614

Abstract: The introduction of the fifth generation wireless systems caused social emotions regarding the impact of electromagnetic waves on people. Many people who consider themselves to be particularly sensitive to radiation make metal foil head covers (so called "tinfoil hats") to shield their body from radiation. The aim of this paper is to show how effective the "tinfoil hat" really is when applied to base station radiation in a fifth generation telecommunication system. It presents the results of investigation on effectiveness of these protections in terms of their shielding properties at the frequencies used in fifth generation wireless systems. The research was carried out based on computer simulations. Remcom XFdtd software (software: XFdtd version 7.8.1 manufacturer: Remcom, 315 South Allen Street, Suite 416 State College, PA, USA) utilizing a finite difference time domain method and a numerical model of the head was applied to obtain the data on shielding properties of conductive head covers. It was found that in the case of foil head covers the maximum reduction factor of power density in the head region is approximately 50%. Furthermore, the application of a metal surface shield increases the maximum value of energy absorbed by human tissue in some regions of the head. To overcome this problem, the design of a wire-based shielding structure that does not reduce user comfort is presented as an alternative to the full-metal head cover. For wave propagation in the horizontal plane, its performance is comparable to tinfoil-like structure, but its design makes it much more comfortable for the user.

Keywords: bioelectromagnetics; 5G; FDTD; human body model; shielding; SAR

check for updates

Citation: Januszkiewicz, Ł. Analysis of Shielding Properties of Head Covers Made of Conductive Materials in Application to 5G Wireless Systems. *Energies* **2021**, *14*, 7004. https://doi.org/10.3390/en14217004

Academic Editors: Sangheon Pack, Antonio Cano-Ortega and Mauro Feliziani

Received: 20 July 2021
Accepted: 19 October 2021
Published: 26 October 2021

Publisher's Note: MDPI stays neutral with regard to jurisdictional claims in published maps and institutional affiliations.

Copyright: © 2021 by the author. Licensee MDPI, Basel, Switzerland. This article is an open access article distributed under the terms and conditions of the Creative Commons Attribution (CC BY) license (https://creativecommons.org/licenses/by/4.0/).

1. Introduction

Recently, a growing interest in the issues related to the influence of electromagnetic (EM) waves on the human body has been observed. This subject is especially important for people who feel fear of the effects of EM radiation emitted by wireless communication systems, which applies in particular to fifth generation (5G) systems [1]. This is caused mainly by a visible change in the telecommunication infrastructure that requires placing new base station equipment for this new generation of wireless system. These situations may cause the development of irrational behavior in a certain group of people, which are the subject of research by psychologists [2]. Many of these people consider themselves to be particularly sensitive to radiation and seek a way to minimize their exposure to EM fields. As a result of these fears, they fabricate by themselves and use improvised head covers made of conductive materials such as thin aluminum foil [3]. The purpose of this so-called "tinfoil hat" is to protect the user against electromagnetic fields; however, covers of this type are created spontaneously without taking into account the physical phenomena of electromagnetic wave propagation. Often, they are merely the result of a creative reworking of certain observations linking conductive materials to electromagnetic shielding structures.

The research on electromagnetic shields of human body is very challenging because of the problem intricacy. This is due to the complex mechanism of interaction of the electromagnetic wave with the tissues of the human body, which depends on wave parameters

such as frequency and polarization. Moreover, the structures used to be placed close to the body have a complex shape resulting from the use of flexible materials that conform to the shape of the body. In this case, computer simulations can be used. However, they must enable the modeling of both the complex internal structure of the body as well as the thin layers of the conductor placed nearby. This is a task that requires considerable computational effort because thin layers of shielding materials should be mapped using high-resolution discrete models, whose unit cells are not larger than 1 mm. Such models, taking into account even a small area of the body such as the head, require large computing resources, especially in the field of computer memory, in which more than 41 million unit cells should be modeled. Regardless of these difficulties, the problem is so significant that it motivated me to conduct the research described in this article.

The motivation for conducting the research described in this article came from numerous conversations the author had with people who were particularly concerned about 5G base station radiation and wanted to use tinfoil hats. In the literature, there are no data on improvised head shields effectiveness at the frequencies of 5G systems. With this novel research I wanted to bring the science-based evidence that could be used during such discussions. It shows the effectiveness of metal shields and provides numeric data that illustrate this effect. For this purpose, I used well-established methodology—computer simulation with the FDTD method and a numerical model of the human body.

In the literature, the shielding structures applied for the human body are studied for the case when the cell phone is the source of electromagnetic radiation [4–6], while the development of multipurpose shielding materials assumes a plane wave [7,8]. The research carried out with respect to interactions of electromagnetic waves with the human body shows that both construction and the materials used for the human body shield design influence its performance. In [4], the effects of an electromagnetic field over a virtual model of a human head have been simulated in the frequency range from 900 to 1800 MHz. It was shown that the use of new high-tech nanotextile materials for shielding layers around the human body can reduce the effects of EM fields; however, the material configuration should be chosen properly according to the area of application.

In [5], the shielding of cellular phone radiation with thin metal plates is studied, showing that the thickness and orientation of the plate influences the amount of energy absorbed by the head. The shielding material properties were identified in [6] for a particular mobile phone antenna and in this way the amount of energy absorbed by the human head was reduced. In the papers that focus on shielding material development, composites with improved conductivity are considered for this application. In [7], the electrical conductivity and electromagnetic shielding effectiveness of two biocomposites are studied by experimental testing and numerical models, and in [8], it is for carbonless nanoplate composites. This shows the potential of fiber-based materials in the application to electromagnetic shielding.

For frequency selective protection, various periodic structures are proposed in the literature. These arrangements do not require covering the entire area (in this case the head surface) with conductive material. These shields use dielectric base material and replicated elementary structures made of an electric conductor [9,10]. To fabricate a wearable frequency selective shield, numerous technologies developed for realizing conductive structures of different shapes with textile materials can be applied [11]. The technologies of conductive ink printing or embroidery with conductive yarns used for textile antennas can be used [12]. Additionally, the physical vapor deposition of metals on textile substrates allows for fabrication of conducting structures for the complex shapes [13,14], so it can be applied for this purpose as well. The frequency selective shielding structures that could be fabricated with textile technologies may result with products that are far more comfortable to the user compared to a tinfoil hat because they do not limit the transfer of heat and water, which is important for any material located close to the human body.

This article focuses on the analysis of shielding properties of improvised head covers made of conductive materials ("tinfoil hats"). Those are developed and used by people who

feel they are oversensitive to EM radiation and want to shield their heads from the waves emitted by 5G base stations [1,2]. For this reason, in this research the source of radiation is plane EM wave since those who are afraid of EM fields are not likely to place their head in the proximity of a mobile phone. Moreover, the most probable scenario in this case is the head illumination by the wave propagating from the distant base station in the approximately horizontal direction. The analysis of the interaction of electromagnetic radiation and the tissues of the human body was carried out with the finite difference time domain method (FDTD), which is the preferred method for performing electromagnetic simulations for biological effects from wireless devices [15]. A heterogeneous numerical model of the head was used to simulate the effect of electromagnetic shielding at the frequencies of 5G systems. According to the regulations of the European Union, two frequency ranges are currently allocated for such systems. The 700 MHz band covers the range 694–790 MHz [16]. This band allows relatively large coverage of the wireless system to be achieved even in a complex urban environment. Owing to limited data throughput, it is dedicated mostly for Internet of Things applications where a large number of small-power transmitters are used. The next frequency range covers 3.4–3.8 GHz and provides the parameters required to support a large number of connected devices at the same time [17]. This band can be successfully used in the areas of large cities with a high density of buildings. They can also be used to transmit large amounts of data in real—timee.g., video in the highest resolution. For the purpose of the analysis presented in this paper, bands at 750 and 3600 MHz were considered as the EM wave source, which should be representative for two middle frequencies of 5G systems.

The simulations of a human head exposed to an electromagnetic wave was performed for: (1) the case where no cover was used and (2) the model of applying an improvised conductive cover ("tinfoil hat"). For the 3600 MHz band, a frequency selective shielding structure based on vertical wires was also presented. As a result of the simulations, no significant reduction in power density was observed in the area of the head covered with an improvised electromagnetic shield in the case of exposure to the wave emitted toward the face. The introduction of the shield slightly changes the power density distribution, which is illustrated by the data obtained for the eye region. The reduction of the average value of energy absorbed by tissues was observed. The dipole-based structure proposed in this paper performs comparable to the tinfoil-like structure, but its design makes it much more comfortable for potential use.

2. Materials and Methods

The research on interactions between the human body and the electromagnetic waves requires the utilization of an appropriate numerical method and numerical body models. For the purpose of this research, the Remcom XFdtd computer program was applied [18,19]. It implements the FDTD numerical method that is widely used for electromagnetic simulations of microwave structures fabricated with dielectric materials of complex properties [20,21]. It is especially useful for simulating biological effects from electromagnetic radiation [15]. This method is very efficient in providing accurate results of the field penetration into biological tissues [22,23]. Computer simulation of energy absorbed by body tissues with the FDTD method and numerical model of body is a well established methodology for studying the thermal effect of the interaction of the human body with electromagnetic waves. In [24], the predicted values of absorbed energy were compared to data obtained from an empirical experiment based on measurements with infrared thermography. Comparison between numerical solutions (FDTD) and empirical data showed good agreement. That is why I used this method in further research.

In computer programs that utilize FDTD, models of simulated objects have to be divided into cuboidal elementary cells (voxels) with a side-length not larger than one-tenth of the wavelength in the simulated object. Often, in the case of heterogeneous body models, much smaller voxels are used, which results from the need to reproduce small body structures such as, for example, thin blood vessels or small bones. The simulation of

the entire body with these models requires the use of many elementary cells, and hence the significant hardware resources of the computer, in the memory of which the model is stored and values of wave parameters calculated for all voxels. Heterogeneous anthropomorphic models, especially, when used to simulate interaction with very short waves, require time-consuming computer simulations and may require the use of significant hardware resources (in particular, computer memory). To reduce the simulation time, for this investigation only the model of the human head was used, which is presented in Figure 1. It is a model that was elaborated based on body scans using the magnetic resonance technique at the Hershey Institute [25,26]. The model is provided by the Remcom company to be used with XFdtd software (software: XFdtd version 7.8.1 manufacturer: Remcom, 315 South Allen Street, Suite 416 State College, PA, USA). In this model, tissues are characterized with the Cole–Cole extrapolation technique [27]. Their dielectric parameters for each frequency of interest were taken from the literature [28]. This heterogeneous model consists of 24 different tissue materials divided on 1 mm voxels. In Figure 2, the cross-section of the head model is presented and the tissue materials are indicated with different colors. The width of the model (x direction dimension) is 277 mm, depth (y direction dimension) is 181 mm, and model height (z direction dimension) is 299 mm. The total number of voxels is 7,139,900 and the mass is 7.969 kg. The number of voxels and mass of each tissue are given in Table A1 in Appendix A.

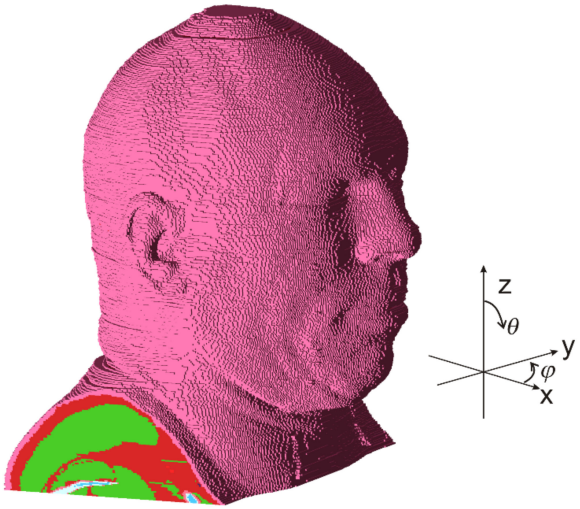


Figure 1. Numerical model of the human head used for simulations.

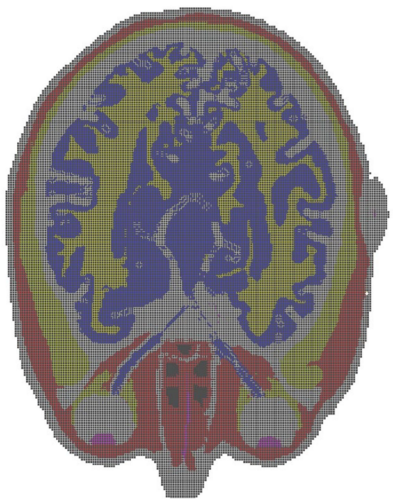


Figure 2. Numerical model cross-section of the head.

The numerical experiments were performed assuming the plane electromagnetic wave as the source of energy. The simulations were made for the frequency equal to 750 MHz and 3600 MHz. The angles of wave incidence φ and θ are defined in Figure 1. The simulations were made for $0^\circ \leq \varphi \leq 180^\circ$ and $0^\circ \leq \theta \leq 90^\circ$ in 30° steps. The wave was linearly polarized in vertical direction (parallel to z axis).

The maximum level of exposure of an electromagnetic field is regulated by Polish law [29] that is harmonized with European Union regulations. According to this, the general population exposure limit for electric field strength at 750 MHz is 37.6 V/m and 61 V/m for 3600 MHz. For the purpose of further analysis, the exposure level for the upper band was applied in simulations (61 V/m) so that the results obtained for the two bands could be easily compared.

The model of the human head presented in Figures 1 and 2 was used as the reference because it does not include any shielding. The improvised metallic shield (tinfoil hat) was modeled with an ellipsoidal shape structure surrounding the human head, forming a metal surface shield (see Figure 3). The electric conductivity of shield is assumed to be the same as for aluminum ($\sigma = 2.5 \times 10^7$ S/m).

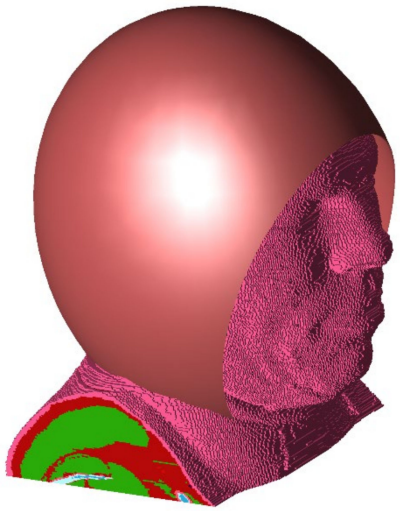


Figure 3. Model of head with metal surface shield.

In the literature, many structures are presented that were developed for the purpose of frequency selective shielding [10,30,31]. They are created with multiple conducting elements of complex shape that are tuned to absorb energy of the wave at a particular frequency. This concept can be applied to the head shields that in this case could be fabricated with textile technologies. They do not cover entire head with an electric conductor, such as aluminum foil, and could be potentially fabricated with conductive fibers integrated with clothing.

In further research, I wanted to verify if a very simple structure that consists of a set of conducting elements can shield the head from electromagnetic fields in the comparable level to solid metal shields. I assumed that the frequency for this shield was 3600 MHz because this is the band for which higher data throughput is possible and the greater utilization is expected as well as power radiated by the equipment. Considering the limitations of textile technologies, in which long or complex conductive structures can be broken due to material flexibility [32], I was searching for the structure of the simplest possible geometry.

The wire-based shield proposed here utilizes the concept of a receiving dipole antenna loaded with the resistor. It is presented in the Figure 4a. The dipole antenna couples to the electromagnetic wave and, if loaded, absorbs the energy of the electromagnetic wave. Since the textile technology of shield fabrication was assumed here, I did not utilize a perfectly conducting dipole loaded with a single resistor, but instead a wire element that

is fabricated with an electric conductor of limited conductivity (lossy), as presented in Figure 4c. It acts similarly to an antenna fabricated with many resistors distributed along its length, presented in Figure 4b [33]. For this structure, it is difficult to predict the resonant length because the velocity of current propagation along the structure differs with element conductivity. If a set of wires is considered, the coupling between wires also depends on their distance, influencing the performance of the structure. To verify if the set of lossy wires can be used for shielding purposes, I used a sample configuration of a four-element array, which is presented in Figure 5. The limited number of elements was used to improve numerical efficiency of the experiment. To identify the length L and the conductivity σ of the wires, the simulations of power density behind the wires were performed. I used brute-force scan of element length and element conductivity to identify which combination gives promising results. I made the simulations for all combinations in the range of L from 30 to 60 mm, every 1 mm, and for values of σ: 200, 500 and 1000 S/m. The distance between wires was set to D = 10 mm and the wire diameter was 1 mm, so the structure could be fabricated with embroidery technique as well as with ink-jet printing on textile substrate. The array was illuminated by a vertically polarized plane wave at 3600 MHz and electric field intensity Ez = 61 V/m. The test point was located at x = 5 mm, y = 0 and z = 0. The sample results obtained for different wire length and conductivity are presented in Table 1. For simplicity, only the data for the shortest, locally optimal length (L = 47 mm) and the longest wire are presented.

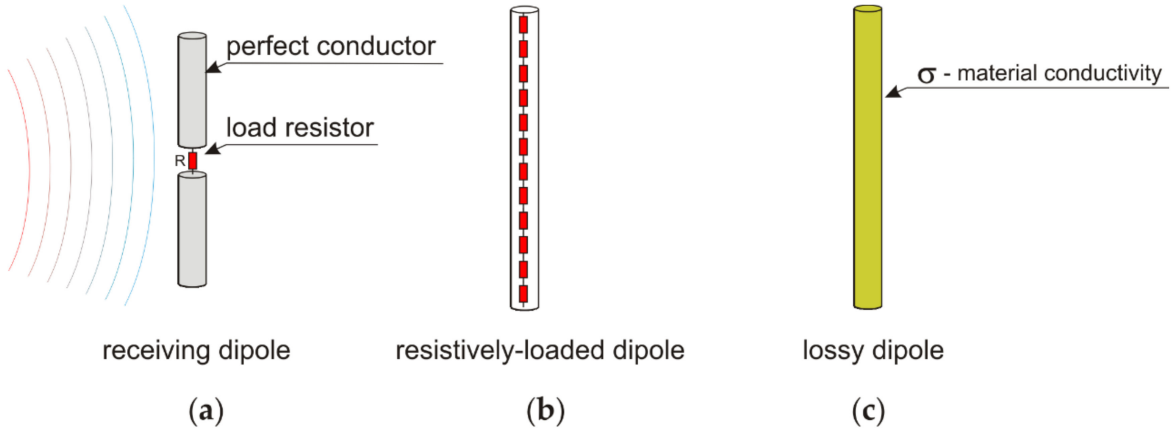


Figure 4. The evolution of the shielding element concept, from loaded receiving dipole to lossy dipole: (**a**)—dipole loaded with single resistor, (**b**)—dipole loaded with set of resistors, (**c**)—dipole made of lossy material.

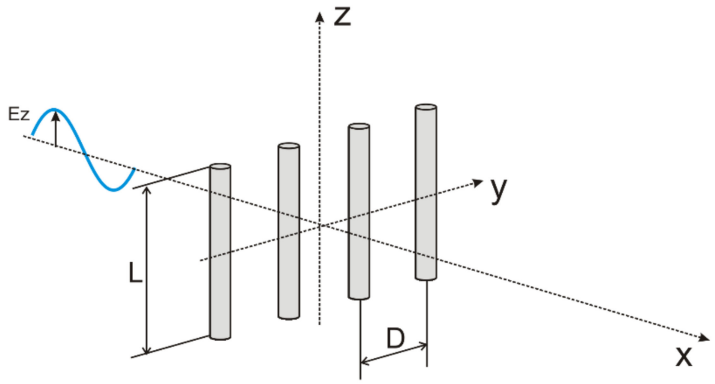


Figure 5. Geometry of four wire array.

Table 1. Power density at the test point (x = 5 mm, y = 0, z = 0) located behind the four wire array.

L (mm)	σ (S/m)	S (W/m^2)
30	200	6.5
30	500	7.2
30	1000	7.6
47	200	0.68
47	**500**	**0.47**
47	1000	0.52
60	200	3.03
60	500	3.33
60	1000	3.5

The lowest value of power density level (0.47 W/m^2) was obtained for the length of wires equal to 47 mm and conductivity of 500 S/m. The power density distribution (in logarithmic scale with reference to 10 W/m^2) obtained for this case is presented in Figure 6 for the x–z plane and in Figure 7 for the x–y plane (z = 0). The color level in the figures corresponds to the power density. Red indicates the region where the power density is not less than 10 W/m^2, while dark blue indicates places where the power density is below −35 dB, referring to 10 W/m^2 (that is 3.2 mW/m^2). This color scale is also used in later figures that present power density.

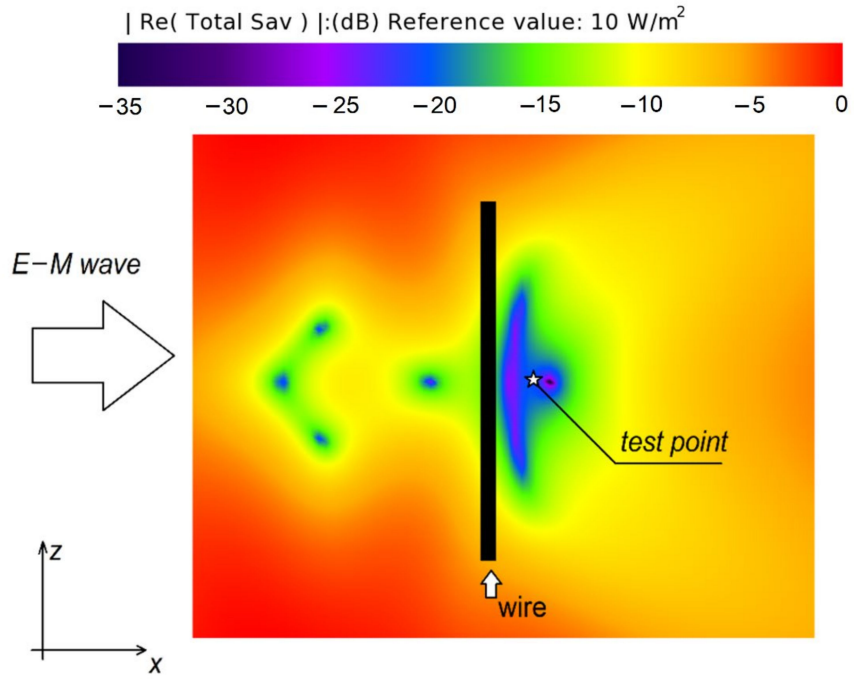


Figure 6. Power density distribution in the $x - z$ (y = 0) plane for the four wire array (the length of wires: 47 mm, conductivity: 500 S/m). Values given in logarithmic scale with reference value 10 W/m^2.

This simple configuration of conducting wires reduces locally the power density from 10 to 0.47 W/m^2. It was used as the initial design of the wire-based head shield because it can be easily manufactured with textile technologies such as printing with conductive ink or embroidery with conductive yarns and then can be incorporated into the clothes. In Figure 8, the simplified model of the wire-based head shield is presented. This is formed with the set of vertically aligned wires of length equal to 47 mm and conductivity of 500 S/m. The wires have the same diameter as in the four-element case (1 mm) and are located at the same distance (10 mm apart from each other). This is a simplified model

to verify the possible applicability of this concept to human head shielding. It does not imitate the final wire alignment that is on the surface of flexible textile material.

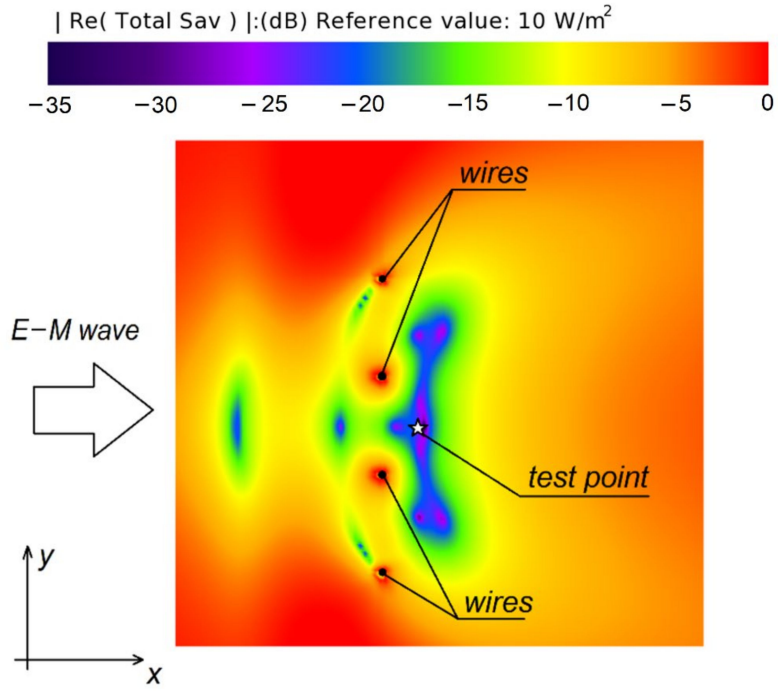


Figure 7. Power density distribution in the $x - y$ ($z = 0$) plane for the four wire array (the length of wires: 47 mm, conductivity: 500 S/m. Values given in logarithmic scale with reference value 10 W/m^2.

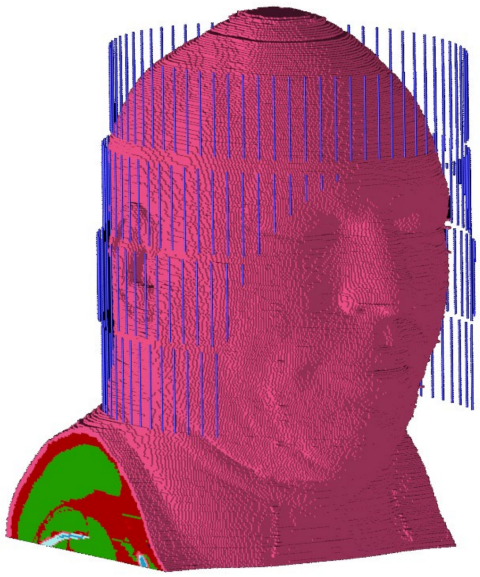


Figure 8. Model of head with wire shield.

3. Results

The simulations with the abovementioned models were performed to make the comparative study of shielding properties of conductive structures.

The power density distribution resulting from an incident wave from the distant base station was simulated (the direction of propagation is in this case approximately horizontal). The results are presented at the cross-section of the model in the x–y plane at the eye level. The wave incidence angle was $\varphi = 0°$, $\theta = 90°$. The reference results for the uncovered head

obtained for 750 MHz are presented in Figure 9. Figure 10 presents corresponding data for the head covered with the metallic surface shield. In Figures 9 and 10, power density is presented in the logarithmic scale (in dB) with the reference value equal to 10 W/m^2.

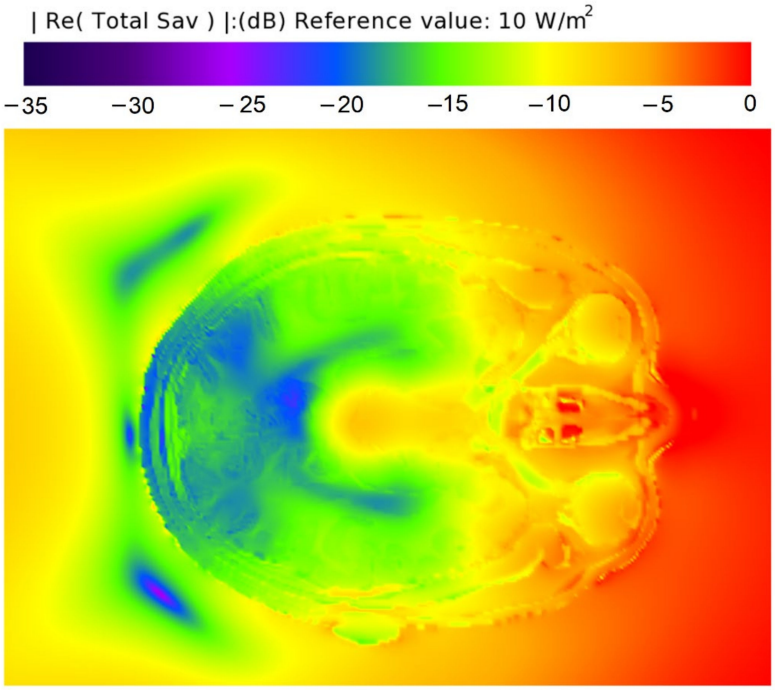


Figure 9. Power density for uncovered head, 750 MHz (in the logarithmic scale with reference value equal to 10 W/m^2).

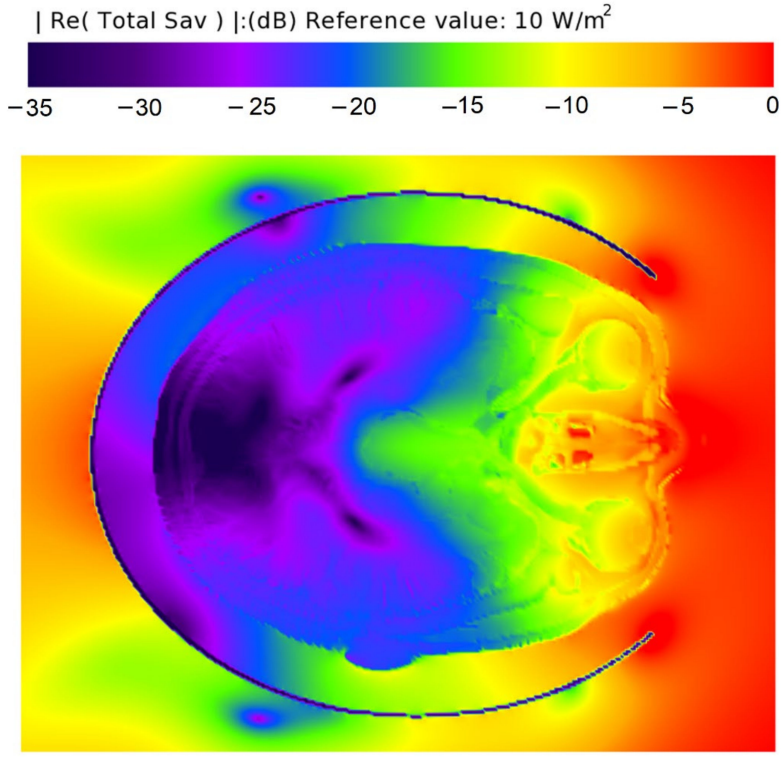


Figure 10. Power density for metal surface shield, 750 MHz (in the logarithmic scale with reference value equal to 10 W/m^2).

The power density for the frequency of 3600 MHz and the uncovered head is presented in Figure 11. Figure 12 presents corresponding data for the head covered with the metal surface shield. The results for the wire shield are presented in Figure 13.

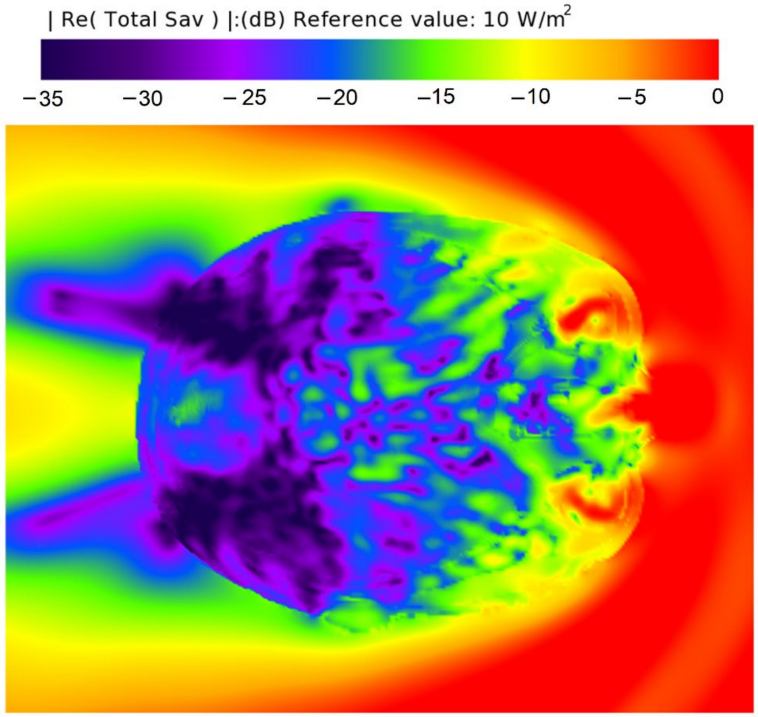


Figure 11. Power density for uncovered head, 3600 MHz (in the logarithmic scale with reference value equal to 10 W/m^2).

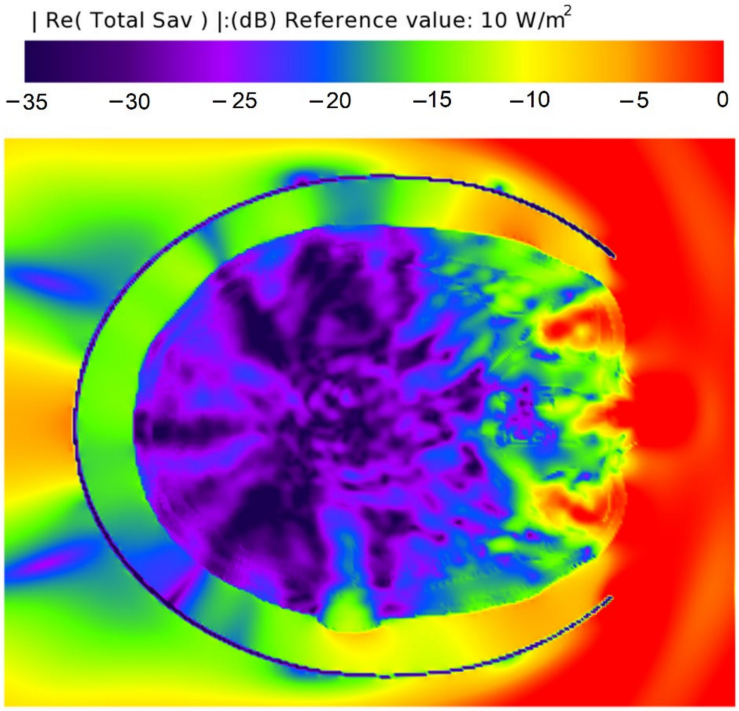


Figure 12. Power density for conductive shield, 3600 MHz (in the logarithmic scale with reference value equal to 10 W/m^2).

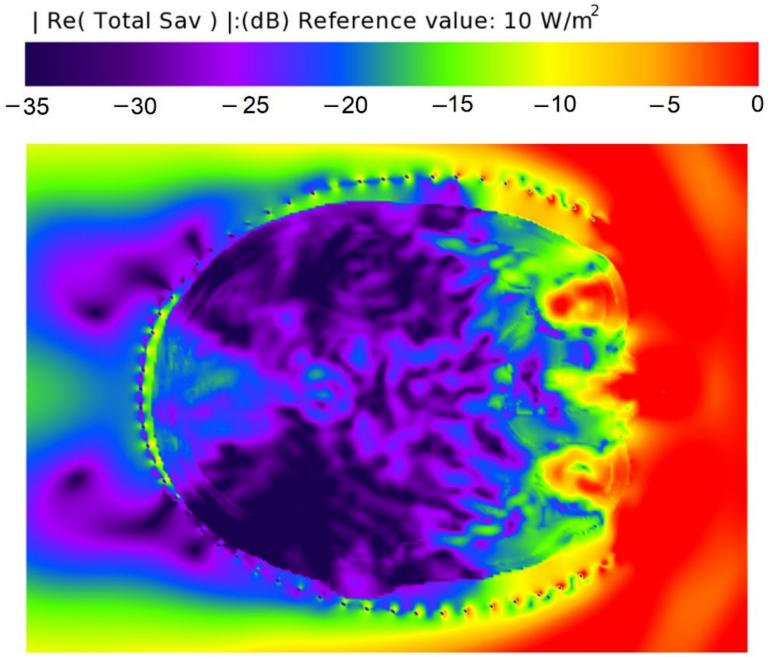


Figure 13. Power density for wire shield, 3600 MHz (in the logarithmic scale with reference value equal to 10 W/m^2).

The specific absorption rate (*SAR*) is the parameter commonly used to determine the interaction of electromagnetic fields with the human body in terms of absorbed energy by the mass of tissue. This is defined by the following equation:

$$SAR = \frac{\sigma |E|^2}{\rho} \quad (1)$$

where:

σ—electrical conductivity (S/m)
E—electric field strength (V/m)
ρ—tissue density (kg/m^3)

This parameter is often used in various regulations of electromagnetic field exposure limits, defined in terms of *SAR* averaged over a volume of tissue. Typically, *SAR* is averaged in 10 g and in 1 g of tissue. The simulations of *SAR* were made for $0^\circ \leq \varphi \leq 180^\circ$ and $0^\circ \leq \theta \leq 90^\circ$ with steps of 30°. The results of *SAR* parameter simulations for the unshielded and shielded head are presented in Table 2 for the frequency of 750 MHz and for the most probable case where the base station antenna is far from the user and the wave approaches from horizontal direction ($\theta = 90^\circ$). To simplify the analysis, it was first simulated for three values of wave incidence angle ($\varphi = 0^\circ, 90^\circ, 180^\circ$). Table A2 in Appendix B presents *SAR* for all the combinations of φ and θ angles that were considered. Data presented in Tables 2 and A2 present the maximum and average values of *SAR* averaged in 10 and 1 g of tissues.

Table 2. *SAR* parameters for 750 MHz, for $\theta = 90^\circ$.

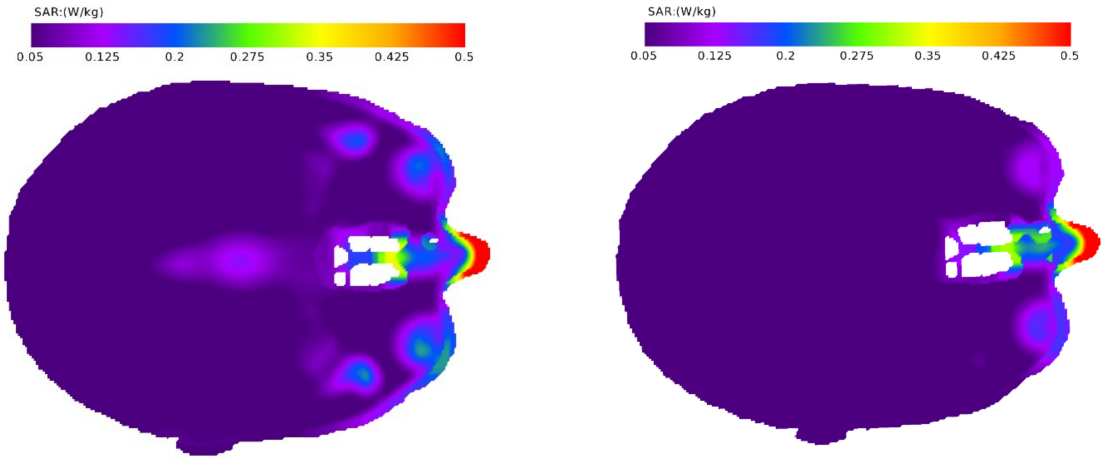
φ Angle (○)	*SAR* Parameter	*SAR* Value No Shield (W/kg)	*SAR* Value Metal Surface Shield (W/kg)
0	10 g averaged, maximum	0.51	0.72
0	10 g averaged, average	0.084	0.058
0	1 g averaged, maximum	0.6	0.92
0	1 g averaged, average	0.084	0.058
90	10 g averaged, maximum	0.425	0.488
90	10 g averaged, average	0.083	0.04
90	1 g averaged, maximum	0.59	1.66
90	1 g averaged, average	0.083	0.04
180	10 g averaged, maximum	0.344	1.0
180	10 g averaged, average	0.082	0.038
180	1 g averaged, maximum	0.634	3.58
180	1 g averaged, average	0.082	0.038

In the Table 3, *SAR* parameters are presented for the frequency of 3600 MHz for a limited number of wave incidence angles φ and for $\theta = 90^\circ$ that correspond with distant transmitter location. In this case, the data obtained for no shield and metal shield are presented together with the results obtained for the wire shield model presented in Figure 8. Table A3 gathers the results of *SAR* simulations for all angles of wave incidence that were considered.

Table 3. *SAR* parameters for 3600 MHz, for $\theta = 90^\circ$.

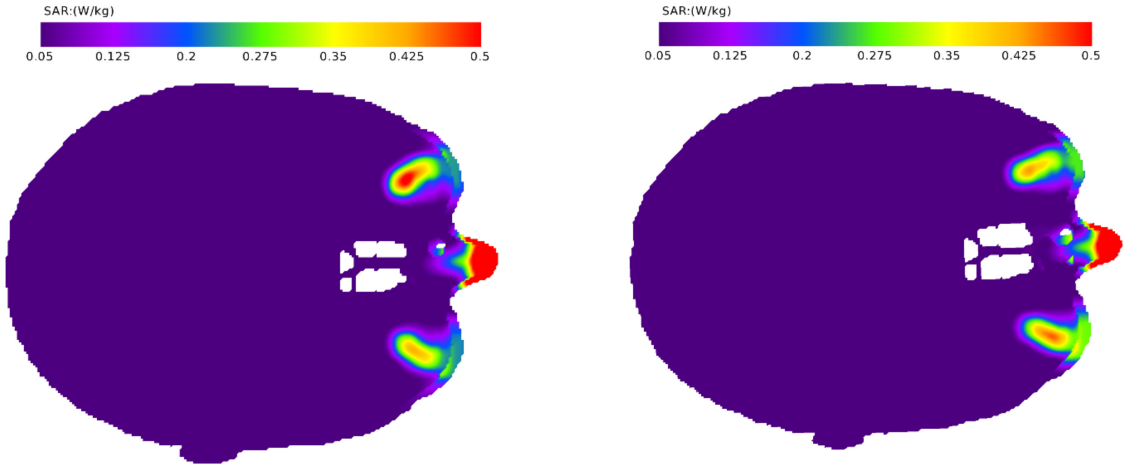
φ Angle (○)	*SAR* Parameter	*SAR* No Shield (W/kg)	*SAR* Metal Surface Shield (W/kg)	*SAR* Wire Shield (W/kg)
0	10 g averaged, maximum	0.454	0.45	0.45
0	10 g averaged, average	0.032	0.024	0.025
0	1 g averaged, maximum	1.02	1	1
0	1 g averaged, average	0.32	0.024	0.024
90	10 g averaged, maximum	0.33	0.53	0.3
90	10 g averaged, average	0.04	0.019	0.023
90	1 g averaged, maximum	0.85	1.18	0.63
90	1 g averaged, average	0.04	0.019	0.023
180	10 g averaged, maximum	0.25	0.3	0.27
180	10 g averaged, average	0.037	0.02	0.025
180	1 g averaged, maximum	0.48	0.55	0.53
180	1 g averaged, average	0.037	0.02	0.025

In Figure 14, *SAR* averaged in 1 g of tissue mass simulated for 750 MHz is presented for the unshielded case (a) and the metal surface shield (b). Figure 15 presents the same parameter for the 3600 MHz shielded and unshielded case. Results obtained for the wire shield that was designed for 3600 MHz are presented in Figure 16. The distribution of the *SAR* parameter presented in those figures was simulated in the *x*–*y* plane at eye level so the position of the plane is the same as for the power density data presented in Figures 8–12. Here, the mass-averaged *SAR* value is given on a linear scale in the range from 0.5 to 0.05 W/kg. The white regions are the volumes of air in nasal auricle and sinuses. The air does not introduce the energy loss; thus, *SAR* is not calculated there.



(**a**) (**b**)

Figure 14. *SAR* averaged in 1 g of tissue mass simulated for 750 MHz: (**a**) no shield and (**b**) metal surface shield.



(**a**) (**b**)

Figure 15. *SAR* averaged in 1 g of tissue mass simulated for 3600 MHz: (**a**) no shield and (**b**) with metal surface shield.

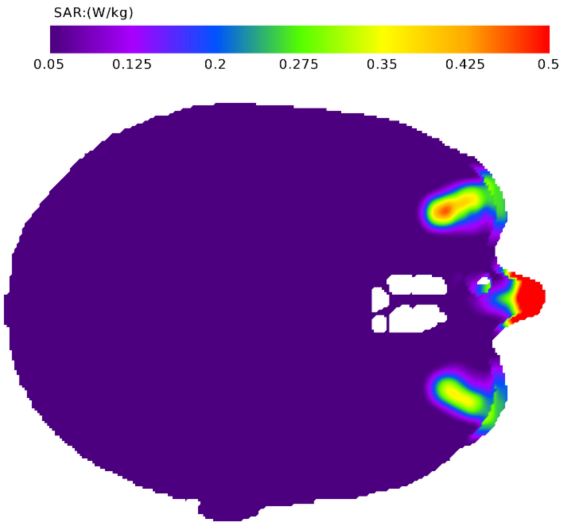


Figure 16. *SAR* averaged in 1 g of tissue mass simulated for 3600 MHz, wire shield.

4. Discussion

The results of computer simulations presented above make it possible to estimate the effectiveness of head shields made of conductive materials. Their shielding properties can be verified by comparing the exposure parameters of the body obtained with the uncovered head model and the head surrounded by a shielding structure.

In the case of the power density analysis for the head area, no major differences were found between the model with the shield and the model uncovered. For the angle of exposure $\varphi = 0^\circ$ and $\theta = 90^\circ$ (front illumination) and for the frequency of 750 MHz, the effect of EM wave attenuation in the human head is visible even without additional cover. For the case of the head without cover (Figure 5), the power density has the greatest values for the face region; that is, the side illuminated directly by the wave. In the region of the left eye, the maximum power density varies from 3 to 1 W/m^2. The power density in the back of the head is lower due to the attenuation in tissues. In the region of the cerebral cortex at the back of the brain, the power density is approximately 0.3 W/m^2. In the model of the tinfoil hat (Figure 6), a similar effect is visible; however, power density in the back of the head was additionally decreased. This effect applies to the very low power density range, which is more than 10 dB smaller than the levels on the side exposed to radiation. Therefore, it has no significant influence on limiting the maximum radiation level in the head area. In the region of the left eye, the maximum power density varies at a similar level to the uncovered case: from 3.1 to 0.7 W/m^2. In the region of the cerebral cortex at the back of the brain, the power density is smaller than in the uncovered case, approximately 0.01 W/m^2.

The differences between the shielded and unshielded case are also not very spectacular in terms of power density for 3600 MHz. Here, for the uncovered case (see Figure 7), in the region of the left eye, the maximum power density varies from 0.3 to 16 W/m^2, while for the metallic shield it varies from 0.2 W/m^2 to 12 W/m^2.

The presence of the conductive shield changes the power density distribution in the proximity of the face. In the region of the eye lens, in the uncovered case the maximum power density is approximately 6 W/m^2. For the shielded model, it has greater value and is equal to 7.3 W/m^2 in the left side of the eye lens. This means that the conductive screen caused a local increase in the power density in the human body, which is an undesirable effect. Additionally, for 3600 MHz, the metal shield decreases the power density in the region of the cerebral cortex at the back of the brain, from 0.12 to 0.04 W/m^2.

A very simple shielding structure designed with conducting wires (presented in Figure 4) has similar performance to the metal surface shield. The results of the power density simulation obtained for this case, presented in Figure 9, are similar to the results for the metallic surface shield (presented in Figure 8). For the shielding structure made with wires in the region of the left eye, the maximum power density varies from 0.45 to 14 W/m^2, while for the region of the cerebral cortex at the back of the brain it is 0.06 W/m^2.

The results of *SAR* simulations were gathered to verify the performance of the shield for different angles of wave incidence. *SAR* averaged in 10 g and in 1 g of tissue was simulated for unshielded and shielded head. The results obtained for 750 MHz are presented in Tables 2 and A2. For this frequency, the maximum value of *SAR* averaged in tissue mass is greater for the shielded case compared to the unshielded case for all angles that were considered. The average value of *SAR* averaged in tissue mass for entire head (both for 1 and 10 g) is slightly lower for the shielded case, depending on the angle of exposure φ. For EM wave directed toward the back of the head ($\varphi = 180^\circ$), the average value of *SAR* averaged in 10 g of tissue was reduced by the metal surface shield from 0.082 to 0.038 W/kg. The data presented in Table A2 show that shielding effectiveness also depends on the incident angle in the vertical plane, but the shield increased the maximum value of *SAR* and reduced approximately by 50% the average value of *SAR* for all the cases considered.

The *SAR* simulation results for 3600 MHz frequency are presented in Tables 3 and A3. In this case, data are given for the unshielded model and for the shield

made of metal surface and wires. The maximum values of *SAR* in the case are also slightly greater for the metal surface shield compared to the unshielded case, but this effect is less significant than for 750 MHz. The simple shield made of vertical wires reduces the energy absorbed by the head for a vertically polarized wave that illuminates the head with an incidence angle θ that has its value close to 90°, that is, the case of a distant base station radiating in an almost horizontal plane. For $\theta = 0°$, shield does not influence the *SAR* parameter. This shield does not cause a noticeable increase of the maximum value. Both shielding structures (metal surface and wire) reduce the average value of *SAR*; however, this effect depends on the angle of exposure. For an EM wave directed toward the left side of the head ($\varphi = 180°$, $\theta = 90°$), the average value of *SAR* averaged in 10 g of tissue was reduced from 0.04 to 0.019 W/kg in the case of the metal surface shield and to 0.023 W/kg for the shield made of wires.

Summarizing these considerations, the following effects can be noticed: the use of a metal surface shield reduces the average *SAR* value but increases the maximum value of this parameter. In addition, locally, it can increase the power density. To investigate this phenomenon, I simulated the current distribution in the horizontal cross-section of the head shielded with the metal surface. Results obtained for 750 MHz are presented in Figure 17 and those for 3600 MHz are given in Figure 18. It can be noted that at the edges of the shield that are close to the face, there is a local increase in current density. The current in the shield is the secondary source of the wave that, together with external excitation (illuminating wave), can at some points increase the power density and *SAR* compared to the unshielded case.

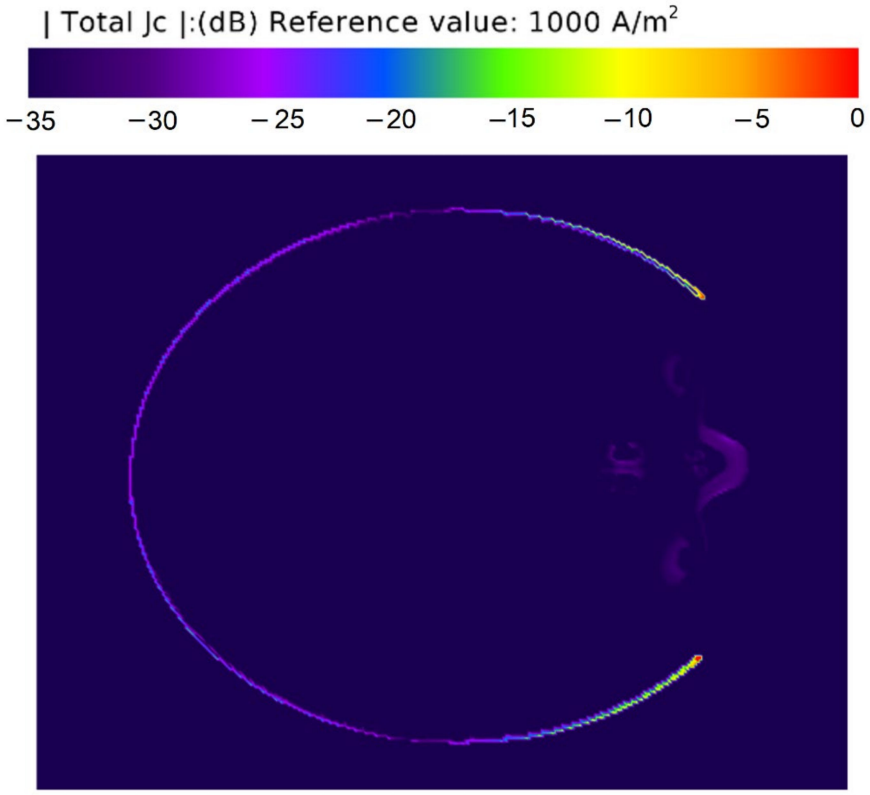


Figure 17. Current distribution for 750 MHz.

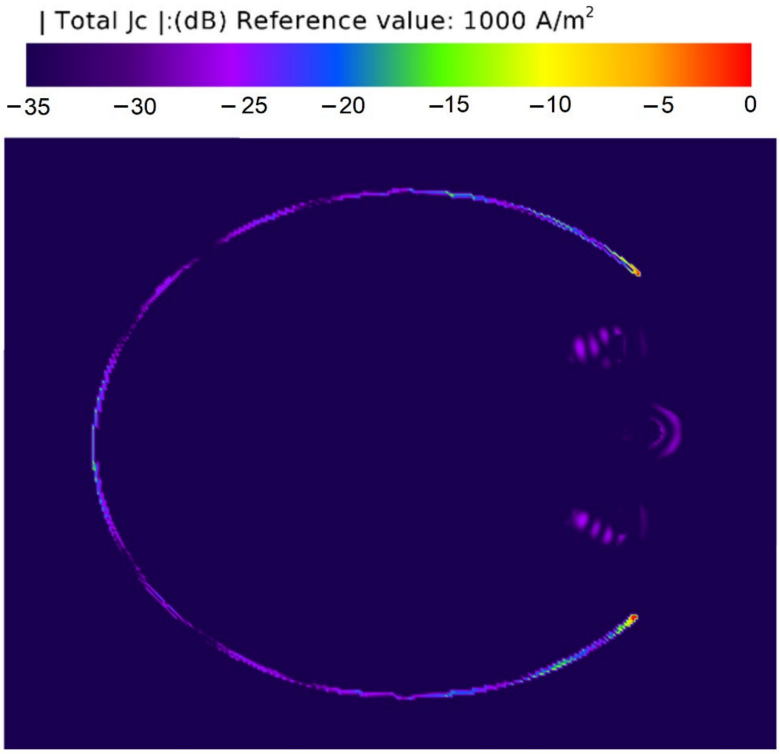


Figure 18. Current distribution for 3600 MHz.

The complex distribution of current in the conducting shield is presented in Figure 19 for the 3600 MHz case. It can be seen that there are many local maxima of current that can increase power density in the body tissues close to the shield.

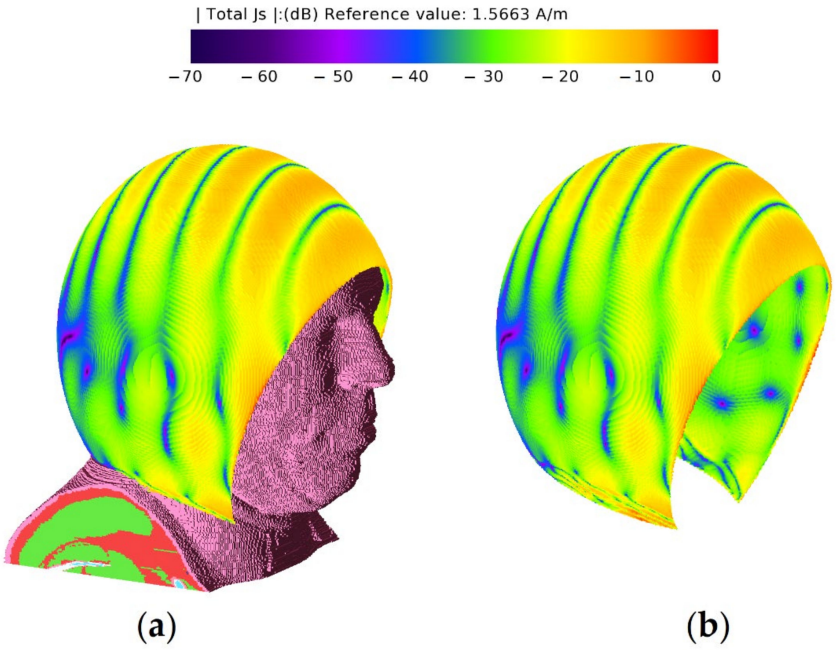


Figure 19. Current distribution in the shield structure for 3600 MHz with the head (**a**) visible and (**b**) not visible.

To analyze the reason for the limited level of shielding, I performed a simulation of the electric field in time domain. For this purpose, instead of sinusoidal excitation that was

used for fixed frequency analysis (750 and 3600 MHz), I used a short pulse, as presented in Figure 20. This short pulse makes possible the analysis of energy propagation in the model. I recorded subsequent distributions of the electric field, which are presented in Table 4. The figures in the table present the electric field distribution on the horizontal cross-section of the human head covered with the metal shield. The wave was propagating from the right side to the left side of the figures. For time t = 0.5 ns, the wave reflected from the face is visible. For t = 0.9 ns, both the wave traveling outside the head cover and inside the cover are visible. When t = 1.5 ns, the wave that was outside the shield is radiated to the left side of the figure, while the part of the energy that was propagating between the head and conducting shield is still in the model. After another fraction of time, for t = 2 ns, it is traveling from the back of the head toward the face. For t = 2.5 ns, it reaches the edge of the shield, and for t = 3 ns, it has left the face region. This analysis shows that for shields made of a solid conductor that has a very large aperture (opening), the energy inserted from the side of the face reaches the back of the shield and is then reflected back. This makes the structure not very effective in terms of limiting the exposition of the human body to the electromagnetic wave energy.

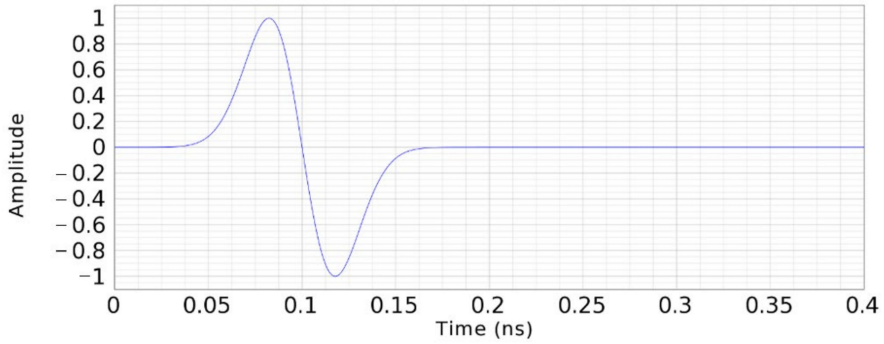


Figure 20. Time domain parameters of the pulse.

Table 4. Electric field intensity for subsequent time steps in a pulse-excited model of a solid metal shield.

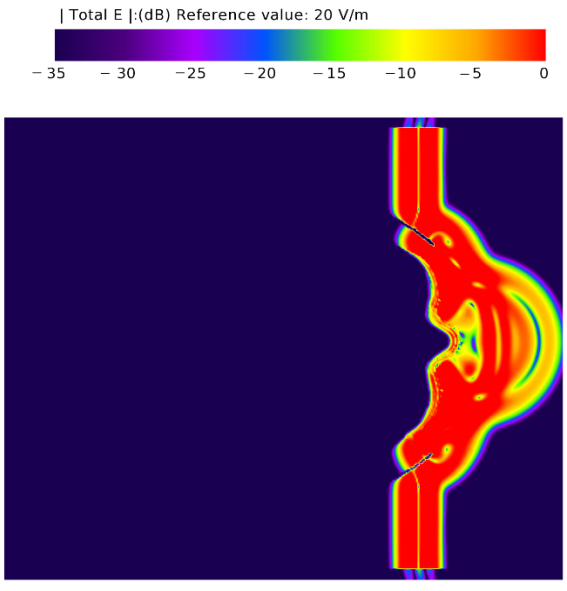
t **(ns)**	***E*** **(V/m)**
0.5	

Table 4. *Cont.*

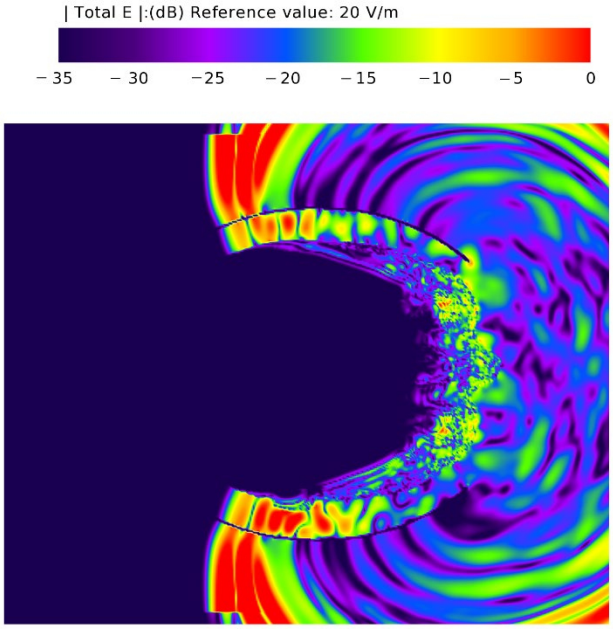
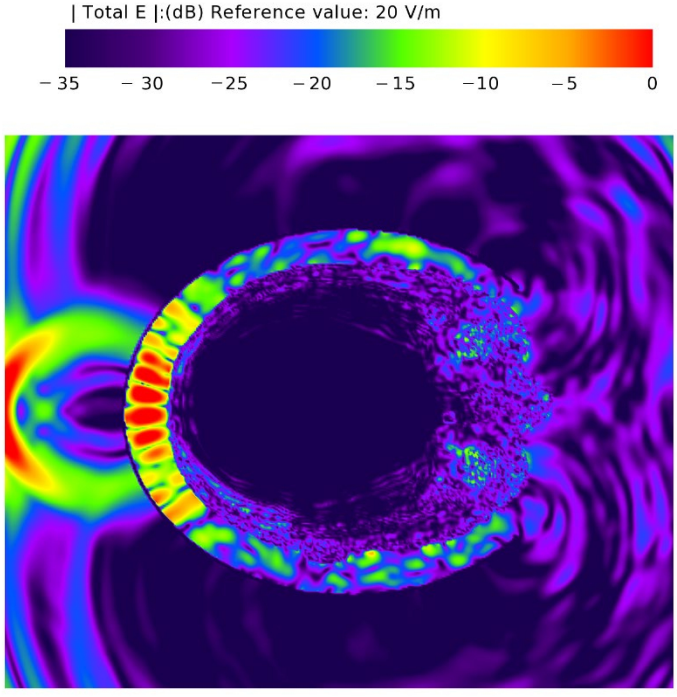
t (ns)	*E* (V/m)
0.9	
1.5	

Table 4. *Cont.*

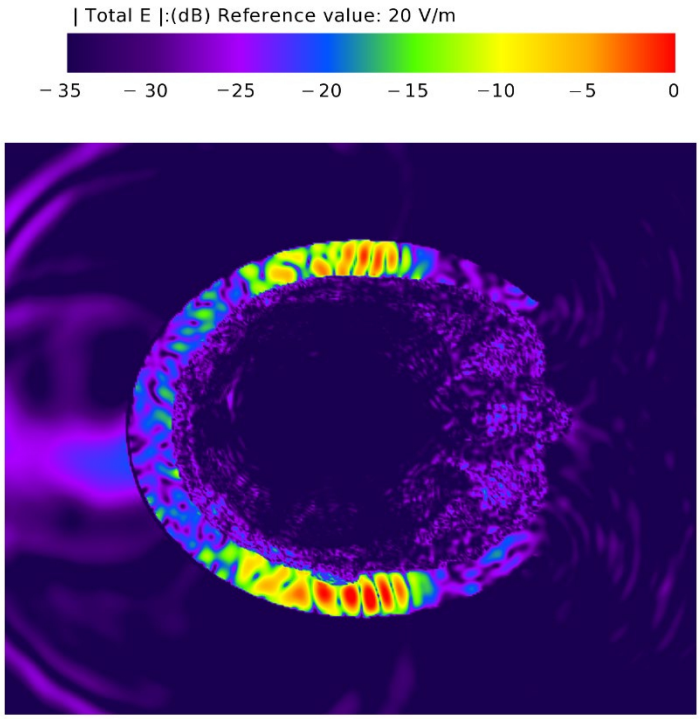
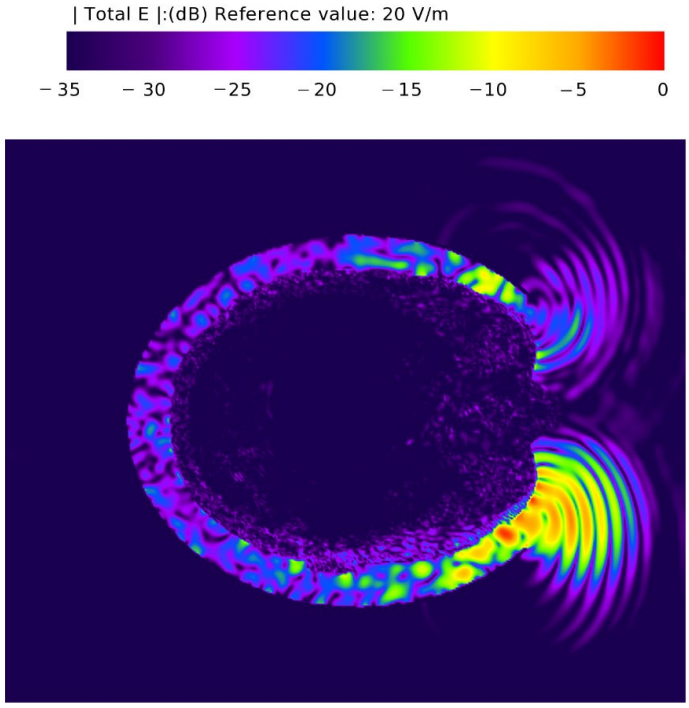
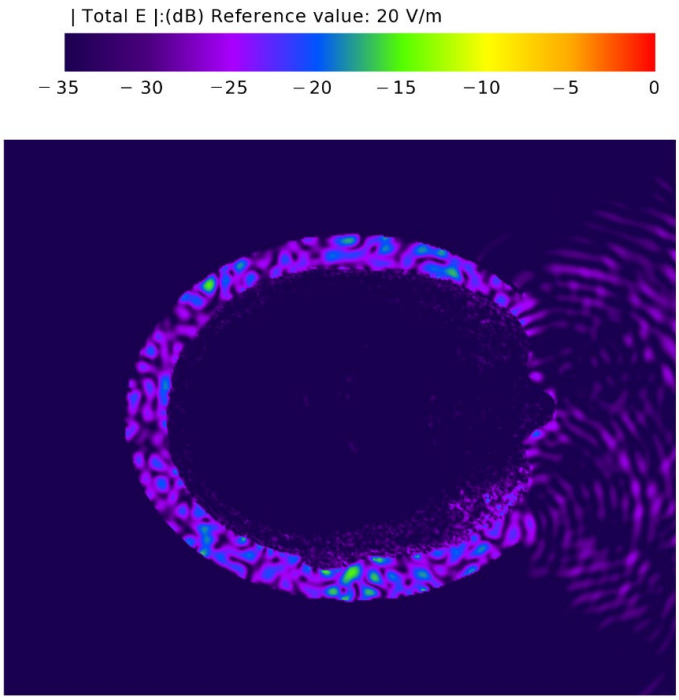
t (ns)	*E* (V/m)
2	
2.5	

Table 4. *Cont.*

t (ns)	*E* (V/m)
3	

5. Conclusions

In this paper, the analysis of shielding properties of improvised head covers made of conductive materials ("tinfoil hats") is presented. The results of computer simulations of a human head exposed to an EM wave similar to fields generated by 5G systems are given. The power density and *SAR* parameters were obtained for the case where no cover was used and the model of an improvised conductive cover was applied. For the 3600 MHz band the frequency, a selective shielding structure based on vertical wires was proposed.

In the case of the wave illuminating the face, no significant reduction in power density was observed in the area of the face and eyes for a head covered with an improvised electromagnetic shield (i.e., full metal shield). Placing the conducting surface close to the body changes the power distribution in the head region. It reduces the power density in the back side of the head, but for some configurations, it may increase power density in the eye lens region.

In the case of conductive screens, which were tested in this study, a limited degree of reduction of the average value of energy absorbed by tissues was observed. This effect, examined with an average value of the *SAR* parameter, depends on the angle of wave propagation. The maximum reduction factor, equal to approximately 50%, was obtained for the metal surface shield for a wave directed to the side of the head. The application of the metal surface shield increases the maximum value of *SAR* compared to the unshielded case.

To a limited extent, the simple dipole-based structure proposed in this paper can be used for frequency selective shielding of the head. For wave propagation in the horizontal plane, its performance is comparable to the tinfoil-like structure, but its design makes it much more comfortable for the user. Such shields that are not fabricated with metal foil do not limit the transfer of heat and water from the body, which is important for any material located close to the skin surface.

Further research will be carried out to investigate different application scenarios, which will include the analysis of shielding performance in other systems such as DVB-T or DAB. Additionally, the shielding of mobile terminal radiation will be investigated.

The initial results presented here on a wire-based shield motivate additional investigations on these structures. Owing to it simple design, that is, a set of conducting wires, the shield can be manufactured with textile technologies, such as printing with conductive ink or embroidery with conductive yarns. These shielding materials could then be integrated with clothing.

In further research, a multilayer configuration of a wire shield with rotated elements will also be developed, thereby providing shielding properties for waves of different polarizations (current design is effective only for vertical polarization).

Funding: This research received no external funding.

Data Availability Statement: All simulation results are available upon request (lukasz.januszkiewicz@p.lodz.pl).

Conflicts of Interest: The author declares no conflict of interest.

Appendix A. Human Body Model Properties

Table A1. Human body model parameters.

Nr	Tissue	Number of Voxels	Mass (kg)
1	blood	18,933	0.0200311
2	blood vessel	25,454	0.0264722
3	body fluid	10,748	0.0108555
4	bone marrow	144,568	0.150351
5	cancellous bone	301,298	0.579492
6	cartilage	45,541	0.0499585
7	cerebellum	128,873	0.13377
8	cerebro spinal fluid	162,548	0.163718
9	cortical bone	361,577	0.719538
10	eye cornea	239	0.000257164
11	eye lens	898	0.00137394
12	eye sclera	3320	0.00340632
13	eye vitreoushumor	11,822	0.0119272
14	fat	1,635,230	1.49787
15	glands	95,665	0.100449
16	gray matter	524,953	0.544901
17	ligaments	347,454	0.423906
18	lymph	15,619	0.0162438
19	mucous membrane	174,946	0.181944
20	muscle	2,041,626	2.13739
21	nerve spine	36,430	0.1379143
22	outer lung	125	0.00013125
23	skin	591,141	0.665034
24	tooth	13,198	0.0285077
25	white matter	447,594	0.464696

Appendix B. *SAR* Parameters for All Considered Combinations of Angles

Table A2. *SAR* parameters for 750 MHz and all combinations of φ and θ angles considered.

φ Angle (○)	θ Angle (○)	*SAR* Parameter	*SAR* Value No Shield (W/kg)	*SAR* Value Metal Surface Shield (W/kg)
0	90	10 g average, maximum	0.51	0.72
0	90	10 g average, average	0.084	0.058
0	90	1 g average, maximum	0.6	0.92
0	90	1 g average, average	0.084	0.058
0	60	10 g average, maximum	0.49	0.57
0	60	10 g average, average	0.078	0.048

Table A2. *Cont.*

φ Angle (○)	θ Angle (○)	*SAR* Parameter	*SAR* Value No Shield (W/kg)	*SAR* Value Metal Surface Shield (W/kg)
0	60	1 g average, maximum	0.81	0.87
0	60	1 g average, average	0.078	0.048
0	30	10 g average, maximum	0.53	0.57
0	30	10 g average, average	0.078	0.046
0	30	1 g average, maximum	0.87	1.22
0	30	1 g average, average	0.078	0.046
0	0	10 g average, maximum	0.39	0.90
0	0	10 g average, average	0.082	0.049
0	0	1 g average, maximum	0.61	3.37
0	0	1 g average, average	0.082	0.049
30	90	10 g average, maximum	0.46	0.63
30	90	10 g average, average	0.083	0.056
30	90	1 g average, maximum	0.55	0.88
30	90	1 g average, average	0.083	0.056
30	60	10 g average, maximum	0.41	0.51
30	60	10 g average, average	0.081	0.047
30	60	1 g average, maximum	0.69	0.75
30	60	1 g average, average	0.081	0.047
30	30	10 g average, maximum	0.43	0.48
30	30	10 g average, average	0.080	0.045
30	30	1 g average, maximum	0.73	1.68
30	30	1 g average, average	0.080	0.045
30	0	10 g average, maximum	0.48	1.05
30	0	10 g average, average	0.082	0.046
30	0	1 g average, maximum	0.63	3.86
30	0	1 g average, average	0.082	0.046
60	90	10 g average, maximum	0.34	0.50
60	90	10 g average, average	0.083	0.049
60	90	1 g average, maximum	0.51	0.90
60	90	1 g average, average	0.083	0.049
60	60	10 g average, maximum	0.41	0.55
60	60	10 g average, average	0.083	0.045
60	60	1 g average, maximum	0.59	1.30
60	60	1 g average, average	0.083	0.045
60	30	10 g average, maximum	0.37	0.53
60	30	10 g average, average	0.081	0.040
60	30	1 g average, maximum	0.59	0.85
60	30	1 g average, average	0.63	0.040
60	0	10 g average, maximum	0.38	0.70
60	0	10 g average, average	0.081	0.038
60	0	1 g average, maximum	0.53	2.48
60	0	1 g average, average	0.081	0.038
90	90	10 g average, maximum	0.42	0.48
90	90	10 g average, average	0.083	0.04
90	90	1 g average, maximum	0.59	1.66
90	90	1 g average, average	0.083	0.04
90	60	10 g average, maximum	0.44	0.59
90	60	10 g average, average	0.084	0.042
90	60	1 g average, maximum	0.58	2.15
90	60	1 g average, average	0.084	0.042
90	30	10 g average, maximum	0.38	0.61
90	30	10 g average, average	0.081	0.035
90	30	1 g average, maximum	0.51	2.18
90	30	1 g average, average	0.081	0.035
90	0	10 g average, maximum	0.44	0.46
90	0	10 g average, average	0.080	0.035
90	0	1 g average, maximum	0.75	0.82
90	0	1 g average, average	0.080	0.035
120	90	10 g average, maximum	0.42	0.84
120	90	10 g average, average	0.079	0.035
120	90	1 g average, maximum	0.57	2.93
120	90	1 g average, average	0.079	0.035
120	60	10 g average, maximum	0.48	1.05
120	60	10 g average, average	0.086	0.042

Table A2. *Cont.*

φ Angle (○)	θ Angle (○)	*SAR* Parameter	*SAR* Value No Shield (W/kg)	*SAR* Value Metal Surface Shield (W/kg)
120	60	1 g average, maximum	0.72	3.6
120	60	1 g average, average	0.086	0.042
120	30	10 g average, maximum	0.43	0.92
120	30	10 g average, average	0.085	0.037
120	30	1 g average, maximum	0.64	3.24
120	30	1 g average, average	0.085	0.037
120	0	10 g average, maximum	0.38	0.80
120	0	10 g average, average	0.080	0.038
120	0	1 g average, maximum	0.63	2.54
120	0	1 g average, average	0.080	0.038
150	90	10 g average, maximum	0.34	1.00
150	90	10 g average, average	0.08	0.036
150	90	1 g average, maximum	0.61	3.48
150	90	1 g average, average	0.08	0.036
150	60	10 g average, maximum	0.43	1.32
150	60	10 g average, average	0.089	0.048
150	60	1 g average, maximum	0.80	4.50
150	60	1 g average, average	0.089	0.048
150	30	10 g average, maximum	0.43	1.05
150	30	10 g average, average	0.088	0.044
150	30	1 g average, maximum	0.68	3.67
150	30	1 g average, average	0.088	0.044
150	0	10 g average, maximum	0.46	1.05
150	0	10 g average, average	0.082	0.046
150	0	1 g average, maximum	0.58	3.59
150	0	1 g average, average	0.082	0.046
180	90	10 g average, maximum	0.34	1.0
180	90	10 g average, average	0.082	0.038
180	90	1 g average, maximum	0.63	3.58
180	90	1 g average, average	0.082	0.038
180	60	10 g average, maximum	0.44	1.23
180	60	10 g average, average	0.090	0.052
180	60	1 g average, maximum	0.86	4.4
180	60	1 g average, average	0.090	0.052
180	30	10 g average, maximum	0.38	0.93
180	30	10 g average, average	0.088	0.047
180	30	1 g average, maximum	0.68	3.42
180	30	1 g average, average	0.088	0.047
180	0	10 g average, maximum	0.39	0.90
180	0	10 g average, average	0.082	0.049
180	0	1 g average, maximum	0.61	3.37
180	0	1 g average, average	0.082	0.049

Table A3. *SAR* parameters for 3600 MHz and all combinations of φ and θ angles considered.

φ Angle (○)	θ Angle (○)	*SAR* Parameter	*SAR* No Shield (W/kg)	*SAR* Metal Surface Shield (W/kg)	*SAR* Wire Shield (W/kg)
0	90	10 g average, maximum	0.45	0.45	0.45
0	90	10 g average, average	0.032	0.024	0.025
0	90	1 g average, maximum	1.02	1	1
0	90	1 g average, average	0.32	0.024	0.024
0	60	10 g average, maximum	0.42	0.44	0.34
0	60	10 g average, average	0.030	0.019	0.028
0	60	1 g average, maximum	0.97	1.0	0.92
0	60	1 g average, average	0.030	0.019	0.028
0	30	10 g average, maximum	0.50	0.45	0.45
0	30	10 g average, average	0.027	0.012	0.031
0	30	1 g average, maximum	1.09	1.13	1
0	30	1 g average, average	0.027	0.012	0.031
0	0	10 g average, maximum	0.38	0.36	0.38
0	0	10 g average, average	0.032	0.012	0.032
0	0	1 g average, maximum	0.98	0.98	1
0	0	1 g average, average	0.032	0.012	0.032
30	90	10 g average, maximum	0.44	0.44	0.46
30	90	10 g average, average	0.035	0.023	0.025

Table A3. *Cont.*

φ Angle (○)	θ Angle (○)	*SAR* Parameter	*SAR* No Shield (W/kg)	*SAR* Metal Surface Shield (W/kg)	*SAR* Wire Shield (W/kg)
30	90	1 g average, maximum	1.23	0.44	1
30	90	1 g average, average	0.035	0.023	0.025
30	60	10 g average, maximum	0.40	0.42	0.38
30	60	10 g average, average	0.033	0.018	0.029
30	60	1 g average, maximum	0.80	0.86	0.78
30	60	1 g average, average	0.033	0.018	0.029
30	30	10 g average, maximum	0.48	0.56	0.42
30	30	10 g average, average	0.031	0.013	0.034
30	30	1 g average, maximum	1.23	1.52	0.99
30	30	1 g average, average	0.031	0.013	0.034
30	0	10 g average, maximum	0.30	0.29	0.30
30	0	10 g average, average	0.032	0.011	0.032
30	0	1 g average, maximum	0.77	0.77	0.8
30	0	1 g average, average	0.032	0.011	0.032
60	90	10 g average, maximum	0.43	0.50	0.44
60	90	10 g average, average	0.040	0.022	0.025
60	90	1 g average, maximum	0.81	1.29	0.85
60	90	1 g average, average	0.040	0.022	0.025
60	60	10 g average, maximum	0.35	0.34	0.31
60	60	10 g average, average	0.038	0.12	0.029
60	60	1 g average, maximum	0.71	0.69	0.68
60	60	1 g average, average	0.038	0.12	0.029
60	30	10 g average, maximum	0.43	0.56	0.32
60	30	10 g average, average	0.036	0.013	0.038
60	30	1 g average, maximum	0.97	1.32	0.67
60	30	1 g average, average	0.036	0.013	0.038
60	0	10 g average, maximum	0.20	0.32	0.25
60	0	10 g average, average	0.034	0.01	0.034
60	0	1 g average, maximum	0.45	0.77	0.55
60	0	1 g average, average	0.034	0.01	0.034
90	90	10 g average, maximum	0.33	0.53	0.3
90	90	10 g average, average	0.04	0.019	0.023
90	90	1 g average, maximum	0.85	1.18	0.63
90	90	1 g average, average	0.04	0.019	0.023
90	60	10 g average, maximum	0.37	0.42	0.32
90	60	10 g average, average	0.040	0.015	0.029
90	60	1 g average, maximum	0.68	1.20	0.80
90	60	1 g average, average	0.040	0.015	0.029
90	30	10 g average, maximum	0.38	0.49	0.34
90	30	10 g average, average	0.038	0.012	0.039
90	30	1 g average, maximum	0.72	1.08	0.97
90	30	1 g average, average	0.038	0.012	0.039
90	0	10 g average, maximum	0.20	0.27	0.30
90	0	10 g average, average	0.034	0.01	0.035
90	0	1 g average, maximum	0.40	0.64	0.66
90	0	1 g average, average	0.034	0.01	0.035
120	90	10 g average, maximum	0.29	0.32	0.35
120	90	10 g average, average	0.037	0.018	0.022
120	90	1 g average, maximum	0.67	0.93	0.94
120	90	1 g average, average	0.037	0.018	0.022
120	60	10 g average, maximum	0.33	0.38	0.26
120	60	10 g average, average	0.038	0.014	0.027
120	60	1 g average, maximum	0.64	0.88	0.51
120	60	1 g average, average	0.038	0.014	0.027
120	30	10 g average, maximum	0.32	0.37	0.36
120	30	10 g average, average	0.038	0.01	0.039
120	30	1 g average, maximum	0.69	0.73	1.04
120	30	1 g average, average	0.038	0.01	0.039
120	0	10 g average, maximum	0.20	0.23	0.28
120	0	10 g average, average	0.034	0.01	0.035
120	0	1 g average, maximum	0.51	0.60	0.53
120	0	1 g average, average	0.034	0.01	0.035
150	90	10 g average, maximum	0.27	0.3	0.33
150	90	10 g average, average	0.036	0.02	0.024
150	90	1 g average, maximum	0.52	1.17	0.71
150	90	1 g average, average	0.036	0.02	0.024
150	60	10 g average, maximum	0.28	0.37	0.26
150	60	10 g average, average	0.036	0.015	0.028
150	60	1 g average, maximum	0.51	0.75	0.45
150	60	1 g average, average	0.036	0.015	0.028
150	30	10 g average, maximum	0.28	0.31	0.27
150	30	10 g average, average	0.037	0.014	0.038
150	30	1 g average, maximum	0.70	0.54	0.70
150	30	1 g average, average	0.037	0.014	0.038
150	0	10 g average, maximum	0.30	0.27	0.30
150	0	10 g average, average	0.033	0.012	0.03
150	0	1 g average, maximum	0.76	0.74	0.80
150	0	1 g average, average	0.033	0.012	0.03

Table A3. *Cont.*

φ Angle (○)	*θ* Angle (○)	*SAR* Parameter	*SAR* No Shield (W/kg)	*SAR* Metal Surface Shield (W/kg)	*SAR* Wire Shield (W/kg)
180	90	10 g average, maximum	0.25	0.3	0.27
180	90	10 g average, average	0.037	0.02	0.025
180	90	1 g average, maximum	0.48	0.55	0.53
180	90	1 g average, average	0.037	0.02	0.025
180	60	10 g average, maximum	0.31	0.38	0.30
180	60	10 g average, average	0.036	0.017	0.03
180	60	1 g average, maximum	0.62	0.77	0.55
180	60	1 g average, average	0.036	0.017	0.03
180	30	10 g average, maximum	0.23	0.36	0.27
180	30	10 g average, average	0.037	0.016	0.037
180	30	1 g average, maximum	0.48	0.69	0.51
180	30	1 g average, average	0.037	0.016	0.037
180	0	10 g average, maximum	0.38	0.36	0.38
180	0	10 g average, average	0.032	0.012	0.032
180	0	1 g average, maximum	0.98	0.98	1.03
180	0	1 g average, average	0.032	0.012	0.032

References

1. Pretz, K. Will 5G Be Bad for Our Health? *IEEE Spectr.* **2019**. Available online: https://spectrum.ieee.org/news-from-around-ieee/the-institute/ieee-member-news/will-5g-be-bad-for-our-health (accessed on 20 February 2021).
2. Bowes, S.M.; Costello, T.H.; Ma, W.; Lilienfeld, S.O. Looking under the tinfoil hat: Clarifying the personological and psychopathological correlates of conspiracy beliefs. *J. Pers.* **2021**, *89*, 422–436. [CrossRef]
3. Goldsby, M.; Koolage, W.J. Should You Be Wearing a Tinfoil Hat. In *Conspiracy Theories: Philosophers Connect the Dots*; Greene, R., Robison-Greene, R., Eds.; Open Court Publishing: Chicago, IL, USA, 2020; pp. 179–192.
4. Tomovski, B.; Gräbner, F.; Hungsberg, A.; Kallmeyer, C.; Linsel, M. Effects of Electromagnetic Field Over a Human Body, Sar Simulation with and Without Nanotextile in the Frequency Range 0.9-1.8GHZ. *J. Electron. Eng.* **2011**, *62*, 349–354. [CrossRef]
5. Li, Y.; Zhang, X.; Yu, J.; Wang, Q.; Tan, B. Simulation of EM Field in Head Model and Shielding Effectiveness for Cellular Handset with PIFA. In Proceedings of the 2008 World Automation Congress, Waikoloa, HI, USA, 28 September–2 October 2008; pp. 1–4.
6. Dutta, P.K.; Jayasree, P.V.Y.; Baba, V.S.S.N.S. SAR reduction in the modelled human head for the mobile phone using different material shields. *Hum. Cent. Comput. Inf. Sci.* **2016**, *6*, 44. [CrossRef]
7. Tserpes, K.; Tzatzadakis, V.; Bachmann, J. Electrical Conductivity and Electromagnetic Shielding Effectiveness of Bio-Composites. *J. Compos. Sci.* **2020**, *4*, 28. [CrossRef]
8. Raagulan, K.; Ghim, J.S.; Braveenth, R.; Jung, M.J.; Lee, S.B.; Chai, K.Y.; Kim, B.M.; Lee, J. EMI Shielding of the Hydrophobic, Flexible, Lightweight Carbonless Nano-Plate Composites. *Nanomaterials* **2020**, *10*, 2086. [CrossRef] [PubMed]
9. Sivasamy, R.; Kanagasabai, M.; Baisakhiya, S.; Natarajan, R.; Pakkathillam, J.K.; Palaniswamy, S.K. A Novel Shield for GSM 1800 Mhz Band Using Frequency Selective Surface. *Prog. Electromagn. Res. Lett.* **2013**, *38*, 193–199. [CrossRef]
10. Farooq, U.; Iftikhar, A.; Shafique, M.; Khan, M.; Fida, A.; Mughal, M.; Anagnostou, D. C-Band and X-Band Switchable Frequency-Selective Surface. *Electronics* **2021**, *10*, 476. [CrossRef]
11. Mohamadzade, B.; Hashmi, R.M.; Simorangkir, R.B.V.B.; Gharaei, R.; Rehman, S.U.; Abbasi, Q.H. Recent Advances in Fabrication Methods for Flexible Antennas in Wearable Devices: State of the Art. *Sensors* **2019**, *19*, 2312. [CrossRef]
12. Ali, S.M.; Sovuthy, C.; Imran, M.A.; Socheatra, S.; Abbasi, Q.H.; Abidin, Z.Z. Recent Advances of Wearable Antennas in Materials, Fabrication Methods, Designs, and Their Applications: State-of-the-Art. *Micromachines* **2020**, *11*, 888. [CrossRef]
13. Korzeniewska, E.; Krawczyk, A.; Mróz, J.; Wyszyńska, E.; Zawiślak, R. Applications of Smart Textiles in Post-Stroke Rehabilitation. *Sensors* **2020**, *20*, 2370. [CrossRef] [PubMed]
14. Korzeniewska, E.; Szczęsny, A.; Lipiński, P.; Dróżdż, T.; Kiełbasa, P.; Miernik, A. Prototype of a Textronic Sensor Created with a Physical Vacuum Deposition Process for *Staphylococcus aureus* Detection. *Sensors* **2020**, *21*, 183. [CrossRef] [PubMed]
15. IEEE. *C95.3-2002, Recommended Practice for Measurements and Computations of Radio Frequency Electromagnetic Fields with Respect to Human Exposure to Such fields, 100 kHz to 300 GHz*; IEEE Standards and Coordinating Committee 28 on Non-Ionizing Radiation Hazards; IEEE: Piscataway, NJ, USA, 2002; pp. 1–126.
16. Decision (EU) 2017/899 of the European Parliament and of the Council of 17 May 2017 on the Use of the 470–790 MHz Frequency Band in the Union. *Off. J. Eur. Union* **2017**, *L 138/131*, 131–137.
17. Commission Implementing Decision (EU) 2019/235 of 24 January 2019 on Amending Decision 2008/411/EC as Regards an Update of Relevant Technical Conditions Applicable to the 3400-3800 MHz Fre-quency Band (Notified under Document C(2019) 262). *Off. J. Eur. Union* **2019**, *L 37/135*, 135–143.
18. Luebbers, R. XFDTD and Beyond-from Classroom to Corporation. In Proceedings of the 2006 IEEE Antennas and Propagation Society International Symposium, Albuquerque, NM, USA, 9–14 July 2006; IEEE: Albuquerque, NM, USA, 2006; pp. 119–122.
19. Homsup, N.; Breakall, J. Application of XFDTD and FEKO Program to the Analysis of Planar Antennas. In Proceedings of the 2010 10th International Symposium on Communications and Information Technologies, Tokyo, Japan, 26–29 October 2010; pp. 646–650.

20. Samoi, E.; Benezra, Y.; Malka, D. An ultracompact 3 × 1 MMI power-combiner based on Si slot-waveguide structures. *Photon. Nanostruct. Fundam. Appl.* **2020**, *39*, 100780. [CrossRef]
21. Gindi, M.; Melamed, A.; Malka, D. A four green-light demultiplexer using a multi gallium nitride slot-waveguide structure. *Photon. Nanostruct. Fundam. Appl.* **2020**, *42*, 100855. [CrossRef]
22. Li, J.; Nie, Z.; Liu, Y.; Wang, L.; Hao, Y. Evaluation of Propagation Characteristics Using the Human Body as an Antenna. *Sensors* **2017**, *17*, 2878. [CrossRef]
23. Rahman, M.M.; Hosain, M.K.; Ahmed, S.; Al Azad, M.W. Investigation of Coil Designs for Transcranial Magnetic Stimula-tion on Realistic Head Model. In Proceedings of the 2017 IEEE Region 10 Humanitarian Technology Conference (R10-HTC), Dhaka, Bangladesh, 21–23 December 2017; pp. 279–283.
24. Gajsek, P.; Walters, T.J.; Hurt, W.D.; Ziriax, J.M.; Nelson, D.A.; Mason, P.A. Empirical validation of SAR values predicted by FDTD modeling. *Bioelectromagnetics* **2001**, *23*, 37–48. [CrossRef] [PubMed]
25. Collins, C.M.; Smith, M.B. Spatial resolution of numerical models of man and calculated specific absorption rate using the FDTD method: A study at 64 MHz in a magnetic resonance imaging coil. *J. Magn. Reson. Imaging* **2003**, *18*, 383–388. [CrossRef]
26. Wang, Z.; Lin, J.C.; Vaughan, J.T.; Collins, C. Consideration of physiological response in numerical models of temperature during MRI of the human head. *J. Magn. Reson. Imaging* **2008**, *28*, 1303–1308. [CrossRef] [PubMed]
27. Cole, K.S.; Cole, R.H. Dispersion and Absorption in Dielectrics I. Alternating Current Characteristics. *J. Chem. Phys.* **1941**, *9*, 341–351. [CrossRef]
28. Gabriel, C. Compilation of the Dielectric Properties of Body Tissues at RF and Microwave Frequencies. Air Force Materiel Command, Brooks Air Force Base, Texas: AL/OE-TR- 1996-0037. 1996. Available online: https://apps.dtic.mil/sti/pdfs/ADA303903.pdf (accessed on 24 October 2021).
29. Dz.U. 2019 poz. 2448. Rozporządzenie Ministra Zdrowia z Dnia 17 Grudnia 2019 r. w Sprawie Dopuszczalnych Poziomów pól Elektromagnetycznych w Środowisku. *Dziennik Ustaw*, 19 December 2019.
30. Mannaa, Y.; Aldhaheri, R. Dual-Band Frequency Selective Surface for GSM Shielding in Modern Buildings. *Aljouf Univ. Sci. Eng. J. AUSEJ* **2017**, *4*, 12–17, ISSN: 1658-6670.
31. Koohestani, M.; Perdriau, R.; Ramdani, M.; Carlsson, J. Frequency Selective Surfaces for Electromagnetic Shielding of Pocket-Sized Transceivers. *IEEE Trans. Electromagn. Compat.* **2020**, *62*, 2785–2792. [CrossRef]
32. Stoppa, M.; Chiolerio, A. Wearable Electronics and Smart Textiles: A Critical Review. *Sensors* **2014**, *14*, 11957–11992. [CrossRef] [PubMed]
33. Kim, J.; Kang, W.; Kim, K. A resistive dipole antenna excited by an impulse generator for ultra-wideband radar applications. In Proceedings of the 2010 IEEE Antennas and Propagation Society International Symposium, Toronto, ON, Canada, 11–17 July 2010; pp. 1–4. [CrossRef]